

Influence of martensite morphology on the work-hardening behavior of high strength ferrite–martensite dual-phase steel

Debdulal Das · Partha Protim Chattopadhyay

Received: 22 March 2008 / Accepted: 10 March 2009 / Published online: 4 April 2009
© Springer Science+Business Media, LLC 2009

Abstract This study concerns influence of martensite morphology on the work-hardening behavior of high-strength ferrite–martensite dual-phase (DP) steel. A low-carbon microalloyed steel was subjected to intermediate quenching (IQ), step quenching (SQ), and intercritical annealing (IA) to develop different martensite morphologies, i.e., fine and fibrous, blocky and banded, and island types, respectively. Analyses of work-hardening behavior of the DP microstructures by differential Crussard–Jaoul technique have demonstrated three stages of work-hardening for IQ and IA samples, whereas the SQ sample revealed only two stages. Similar analyses by modified Crussard–Jaoul technique showed only two stages of work-hardening for all the samples. Among different treatments, IQ route has yielded the best combination of strength and ductility due to its superior work-hardening behavior. The influence of martensite morphology on nucleation and growth of microvoids/microcracks has been correlated with the observed tensile ductility.

Introduction

Dual-phase (DP) steels are characterized by a composite microstructure consisting of hard martensite particles dispersed in the soft ferrite matrix [1, 2]. In ferrite–martensite DP steels, soft ferrite ensures high formability, whereas

hard martensite particles provide enhanced strength. DP steels are characterized by a continuous yielding behavior with a low initial flow stress and a high initial work-hardening rate [3, 4]. So far, attention has been devoted in respect of the importance of volume fraction of martensite (V_M) on strength and ductility [3, 5, 6], analysis of strength and elongation based on using rule of mixtures [7], the effect of the mobile dislocations in ferrite matrix on continuous yielding behavior [4], and the influence of martensite morphology on the mechanical properties [8–10]. However, the influence of morphology of martensite on the work-hardening characteristics of the DP steels is yet to be fully established.

Various empirical laws of stress–strain relationship have been used to explain the work-hardening behavior of DP steels [1, 3, 5, 6], among these most popular are Hollomon analysis [11], and Crussard–Jaoul [12, 13] (C–J) analysis [14–18] based on Ludwik [19] and Swift [20] equations, popularly known as differential C–J (D_{C-J}) [14, 15] and modified C–J (M_{C-J}) [16–18] techniques, respectively. Earlier, it has been demonstrated that applicability of Hollomon relationship is limited in analyzing the work-hardening behavior of DP steels [15]; the same has earlier been successfully analyzed either by D_{C-J} [15] or by M_{C-J} [18] techniques. It has also been reported that the M_{C-J} technique is more suitable than the D_{C-J} technique for describing work-hardening behavior of DP steels with varying V_M [3, 17]. Systematic investigations pertaining to the influence of martensite morphology on the work-hardening behavior of DP steels are insufficient till date, which has been particularly focused in this study. An attempt has also been made to identify the suitable morphology of martensite in the high martensitic regime ($V_M > 0.25$) of DP steel that would provide the best combination of strength and ductility.

D. Das (✉) · P. P. Chattopadhyay
Department of Metallurgy and Materials Engineering,
Bengal Engineering and Science University, Shibpur,
Howrah 711 103, India
e-mail: debdulal_das@metal.becs.ac.in

Experimental

Low-carbon microalloyed hot-rolled steel bars (12 mm × 40 mm × 150 mm) were used in this study. The chemical composition of the steel is presented in Table 1. With an aim to develop the DP microstructures with varying martensite morphologies, steel bar specimens were subjected to three different heat-treatment schedules, namely, intermediate quenching (IQ), intercritical annealing (IA), and step quenching (SQ) as illustrated in Fig. 1.

Microstructures of heat-treated specimens etched with 2% nital solution were studied by using optical microscopy (Carl Zeiss: Axiovert 40 MAT). Image analyses were performed on at least ten numbers of digitally acquired optical micrographs of each set of sample using Leica QMetals software in Leica QWin V3 environment to measure volume fraction of the constituent phases. Quantitative analyses of retained austenite content in the specimens were carried out by X-ray diffraction technique using Philips PW 1830 diffractometer using Cu-K α radiation.

The Vickers hardness numbers (VHN) were measured at 30 kgf load, and an average hardness of ten indented fields for a particular sample was reported. The flat tensile specimens conforming to the ASTM standards (ASTM: Vol.03.01:E8M-96) were machined from the heat-treated rolled-bar with their long axis parallel to the rolling direction. Tensile tests were conducted at ambient temperature in a computer-controlled Instron 4204 machine at a crosshead velocity of 0.5 mm/min using extensometer. Standard tensile properties were determined from the recorded load versus elongation data. Three tensile specimens were tested for each type of microstructure, and the average values are reported. The standard errors in the measured strength and elongation values were ± 7 MPa and $\pm 1\%$, respectively. Recorded tensile data sets were analyzed by using the Hollomon, D_{C-J} and M_{C-J} techniques to study the work-hardening behavior.

Tensile fracture surfaces were studied under scanning electron microscope (SEM, Jeol: JSM-5510) to determine the mode of fracture. The SEM micrographs of sub-surface in the necked region, just beneath fracture surface, of the tensile specimens were also studied by using technique outlined by Davis [4] in order to study the sites for the nucleation of microvoids/microcracks.

Table 1 Chemical composition of the investigated steel

Elements	C	Mn	Si	S	P	Al	Cr	V	Fe
Weight (%)	0.12	1.59	0.58	0.014	0.021	0.13	0.60	0.11	Balance

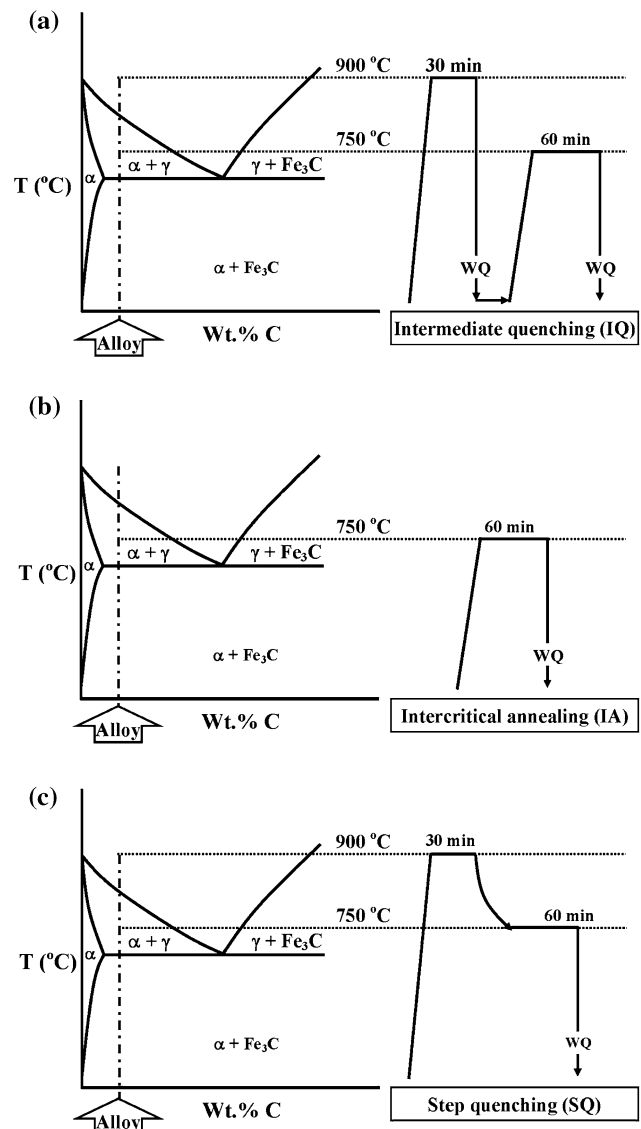


Fig. 1 Schematic presentation of the three kinds of heat-treatment schedules studied: **a** IQ, **b** IA, and **c** SQ. WQ is water quenching

Results and discussion

Microstructural evaluation

Figure 2 shows the optical micrographs of steels subjected to different heat-treatment schedules. It is evident that all the treatments have resulted into ferrite–martensite DP microstructures; however, the shape, size, and distribution of martensite phase vary significantly with the heat-treatment schedules. The IQ specimen has yielded fine and fibrous martensite uniformly distributed in the ferrite matrix (Fig. 2a), whereas SQ specimen reveals blocky and banded ferrite–martensite structure (Fig. 2c) and the IA specimen show martensite inlands along the grain boundaries and triple points of polygonal ferrite grains (Fig. 2b).

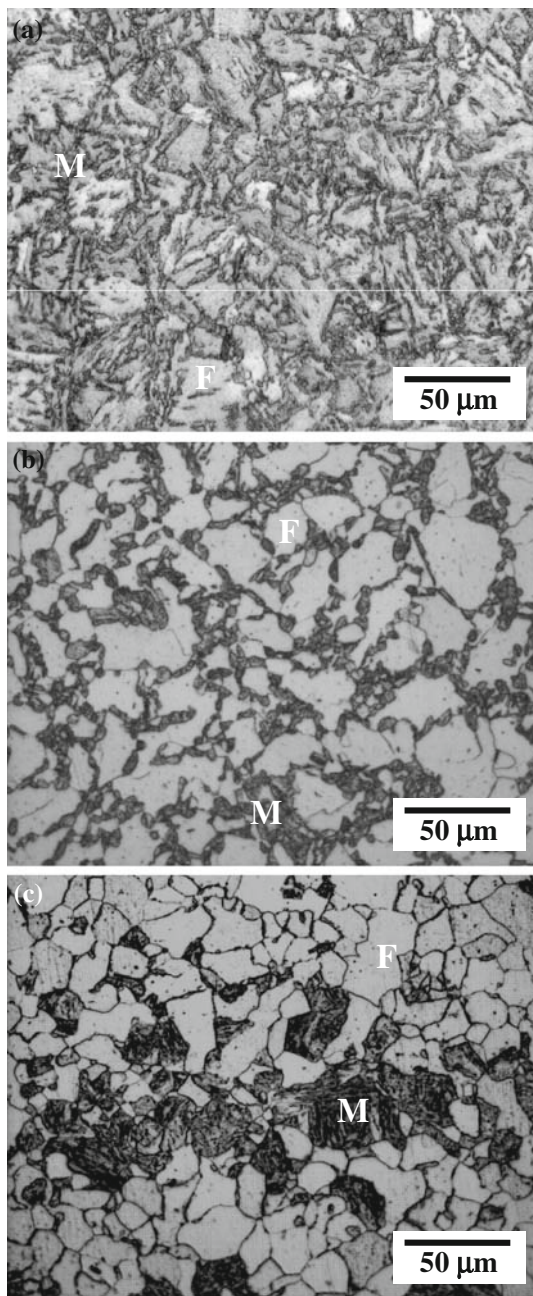


Fig. 2 Optical micrograph of a–c corresponds to the ferrite–martensite DP microstructures obtained in IQ, IA, and SQ treatments, respectively. Samples are etched with 2% nital solution, thus ferrite and martensite phases appear *white* and *black*, respectively. Differences in the morphologies and distribution of martensite phase may be noted

The difference in microstructural state of the sample attained before intercritical treatment may be held responsible for the observed differences in the martensite morphologies [2, 5, 6, 21–23]. In IQ treatment, martensitic structures were intercritically annealed which provides numerous sites for nucleation of both the austenite and ferrite phases [5, 21–23]. The availability of finer and

well-dispersed nucleating sites in large population has resulted into fine and fibrous morphologies of martensite uniformly dispersed in the final DP microstructure (Fig. 2a). In the case of IA treatment, pearlite colonies in the ferrite–pearlite structures of hot-rolled and air-cooled steels occurred in the grain boundaries and triple point regions, which transformed into austenite during subsequent holding at the intercritical region [21, 24]. Those austenite regions transformed into martensite during quenching from the intercritical temperature in the form of islands distributed along the grain boundaries and triple points of ferrite, following the location of pearlite in the initial microstructure. In the case of SQ schedule, single-phase austenite was cooled to the two-phase region where only ferrite nucleates at the grain boundaries of austenite and grows within the austenite grains with appreciable interconnectivities [5, 10, 21–23]. Such a ferrite–austenite structure has resulted into a DP microstructure with alternate bands of ferrite and martensite after quenching from intercritical region.

It is thus evident from Fig. 2 that for a given steel, formation of DP microstructure is governed by the initial microstructure from which the austenite and/or ferrite morphology evolve during annealing in the two-phase region. Image analyses of the micrographs obtained under different schedules with identical intercritical temperature (750 °C) have yielded comparable volume fraction of martensite ($V_M \approx 0.32 \pm 0.04$) for all specimens. Amount of retained austenite in the heat-treated specimens, as measured by X-ray diffraction technique, is insignificant (<2 vol.%) irrespective of the heat-treatment schedules. It may also be mentioned that microstructural studies have not revealed any perceptible presence of carbide or nitride precipitates, which may contribute any significant effect on mechanical properties and work-hardening behavior of the present steel.

Mechanical properties

In general, hardness and strength achieved in the DP microstructures are attributed to the V_M [2, 4, 6, 10]. However, the opportunity of improving the strength of DP steels simply by increasing the V_M has earlier been found to be restricted to $V_M \leq 0.25$ [1, 2, 4]. This has been attributed to the rapid reduction of ductility and toughness of these materials with increasing $V_M > 0.25$ [25, 26]. The more recent investigations have attempted to control the deterioration in ductility at $V_M > 0.25$ by utilizing the influence of martensite morphology on the mechanical properties of high martensitic DP steels [5, 23, 27, 28]. In this study, a $V_M = 0.32 \pm 0.04$ has been achieved by annealing of samples at 750 °C for 60 min with different initial microstructures.

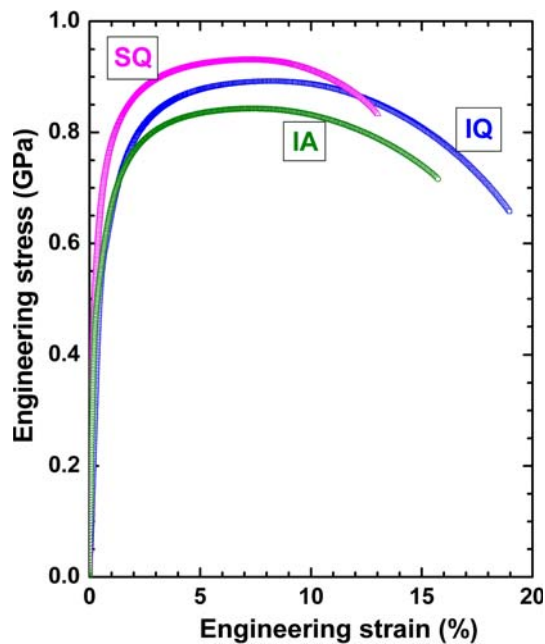


Fig. 3 Engineering stress–strain curve of DP microstructures with varying martensite morphology

Typical engineering stress–strain curves obtained from the tensile testing of the DP steel samples are presented in Fig. 3. It is clear that the stress–strain curves of all the samples present continuous yielding behavior without any notable evidence of yield point phenomenon. Tensile properties, however, varies significantly with the heat-treatment schedules (Fig. 3), which can be attributed to the differences of ferrite–martensite morphologies and their distributions (Fig. 2), since the V_M is nearly same in all the specimens. Among the different samples, IQ sample clearly yields most attractive combination of strength and ductility compared to IA and SQ samples.

Mechanical properties of different DP samples are summarized in Table 2. The results presented in Table 2 assist to infer that among the different samples, the SQ sample exhibits highest hardness, yield, and ultimate tensile strengths, but lowest uniform and total elongation values with less favorable yield ratio and lower level of work-hardening capacity. A comparison of mechanical properties between IA and IQ samples reveals that IQ

sample shows significantly higher values of ultimate tensile strength, total elongation, and magnitude of work-hardening even though the values of hardness, yield strength, and uniform elongation of IQ sample are not considerably superior than those of IA sample. The mechanical properties of DP microstructures with varying martensite morphologies (Table 2) lead to conclude that the fine and fibrous martensite obtained by IQ treatment exhibits intermediate hardness and strength but highest magnitude of work-hardening and ductility; thus yielding the best combination of strength-ductility in the high-martensite regime of DP steel. This observation is in excellent agreement with the reports of Bayram et al. [28] and Bag et al. [5].

Work-hardening behavior

In this study, the work-hardening characteristics of the samples during tensile deformation have been studied in details by carrying out Hollomon as well as differential and modified C-J analyses.

The Hollomon analysis

Earlier analyses of work-hardening based on the Hollomon's equation described the true stress (σ)–true strain (ε) as [11]:

$$\sigma = K\varepsilon^n, \quad (1)$$

where n is the work-hardening exponent and K is the strength coefficient. The Hollomon's plots for the stress–strain data of the present DP microstructures (Fig. 4) exhibit that none of the specimens has followed the linear variation of $\ln \sigma$ versus $\ln \varepsilon$ with unique n value, which is consistent with some earlier reports [1, 6, 15]. The values of n , i.e., slopes of $\ln \sigma$ versus $\ln \varepsilon$ (Fig. 4) at two different ε levels (Table 3), however indicate that (i) rate of work-hardening decreases considerably with increasing deformation for all DP specimens; and (ii) the early stage of deformation which is dominated by deformation of ferrite phase [1–3, 6] is significantly influenced by the morphology of martensite.

Table 2 Summary of mechanical properties of DP microstructures with varying morphology of martensite

Specimen	Hardness (VHN)	Yield strength (MPa)	Ultimate tensile strength (MPa)	Yield ratio ^a	Magnitude of work-hardening ^b (MPa)	Uniform elongation (%)	Total elongation (%)
IQ	266 ± 3	541	892	0.61	351	9.5	19.7
IA	253 ± 6	533	843	0.63	310	8.2	15.8
SQ	281 ± 4	635	931	0.68	296	7.2	13.1

^a Ratio of yield strength to ultimate tensile strength

^b Difference between ultimate tensile strength and yield strength

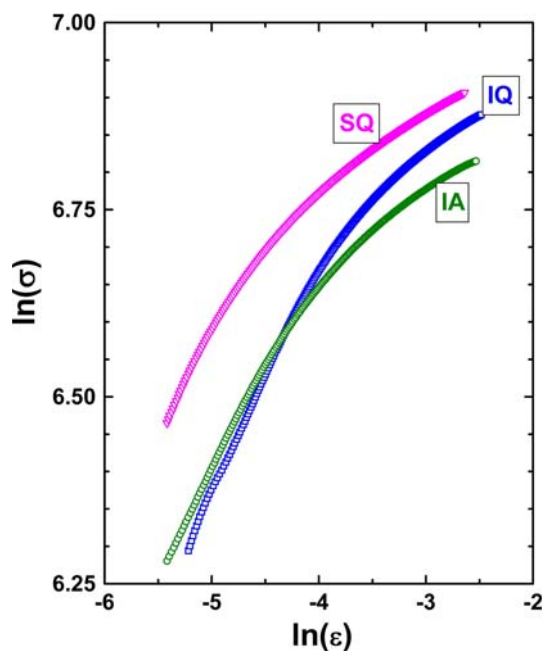


Fig. 4 Holloman’s plot of $\ln(\sigma)$ versus $\ln(\epsilon)$ of ferrite–martensite DP microstructures with varying morphology of martensite

Differential C-J analysis

The differential C-J analysis [14, 15, 29] (D_{C-J}) of work-hardening is based on the power Ludwik relation expressed as [19]:

$$\sigma = \sigma_0 + k' \epsilon^{n'} \tag{2}$$

where n' is work-hardening exponent, and σ_0 and k' are material constants. Equation 2 after differentiation with respect to ϵ is:

$$\ln\left(\frac{d\sigma}{d\epsilon}\right) = \ln(k'n') + (n' - 1) \ln \epsilon \tag{3}$$

The D_{C-J} analyses of tensile data for the different treatments have been carried out using Eq. 3 and the results are shown in Fig. 5. The results reveal three distinctly delineated stages of work-hardening for IQ (Fig. 5a) and IA (Fig. 5b) samples, while only two stages are evident for

the SQ sample (Fig. 5c). In analogy with the earlier reports, three stages of work-hardening in DP steels can be attributed to the following deformation mechanisms [1, 5, 6, 15]:

- Stage-I: Homogeneous deformation of the soft ferrite matrix assisted by the glide of mobile dislocations present near the martensite regions.
- Stage-II: Diminished work-hardening due to the deformation of the constrained ferrite with possible transformation of retained austenite to martensite.
- Stage-III: Simultaneous deformation of ferrite and martensite with attendant cross-slip and dynamic recovery in ferrite.

The values of $(n' - 1)$ at different stages and the transition strains (ϵ_t) from one stage to the next stage for all DP microstructures are summarized in Table 3. The values of $(n' - 1)$ yielded by DP microstructures with different martensite morphologies are different at the stage-I and II, whereas the same in the stage-III are almost comparable. The negative values of $(n' - 1)$ in stage-I and III (Table 3) have been reported earlier for DP steels [9, 14]. For stage-I, this is related to the presence of high internal stress field caused by high density of lattice defect and/or microstructure heterogeneity [9, 14], whereas the same in stage-III is attributed to the attendant cross-slip and dynamic recovery in ferrite [5, 15]. In this study, the magnitude of $(n' - 1)$ varies in the order of $IQ > IA > SQ$ for all the three stages and the differences are more prominent in stage-II (Table 3). In addition, the values of ϵ_t are significantly larger in the case of IQ sample compared to that of IA and SQ samples.

The work-hardening in stage-I deformation of DP steel is related to the initial concentration of mobile dislocations in ferrite phase [5]. Its magnitude is dependent on the availability of ferrite/austenite interface regions prior to quenching that determines the extent of accommodation and distribution of the austenite to martensite transformation stress in ferrite phase. The variations of microstructures (Fig. 2) with different heat-treatment schedules (Fig. 1)

Table 3 Summary of the parameters related to work-hardening behavior of DP microstructures with varying morphology of martensite obtained by different methods

Specimen	Hollomon’s analyses (Eq. 1)		D_{C-J} analyses (Eq. 3)					M_{C-J} analyses (Eq. 5)		
	Slope (n)		Slope ($n' - 1$)			Transition strain, ϵ_t (%)		Slope ($1 - m$)		Transition strain, ϵ_t (%)
	$\epsilon = 0.007$	$\epsilon = 0.05$	Stage-I	Stage-II	Stage-III	Stage-I to II	Stage-II to III	Stage-I	Stage-II	
IQ	0.32	0.08	-2.68	+0.23	-1.54	0.74	1.04	-3.81	-12.03	2.09
IA	0.29	0.08	-2.30	-0.54	-1.44	0.32	0.69	-3.88	-13.75	1.79
SQ	0.28	0.07	-	-0.67	-1.41	-	0.42	-3.48	-11.68	0.92

The standard errors of the different parameters are $\pm 5\%$

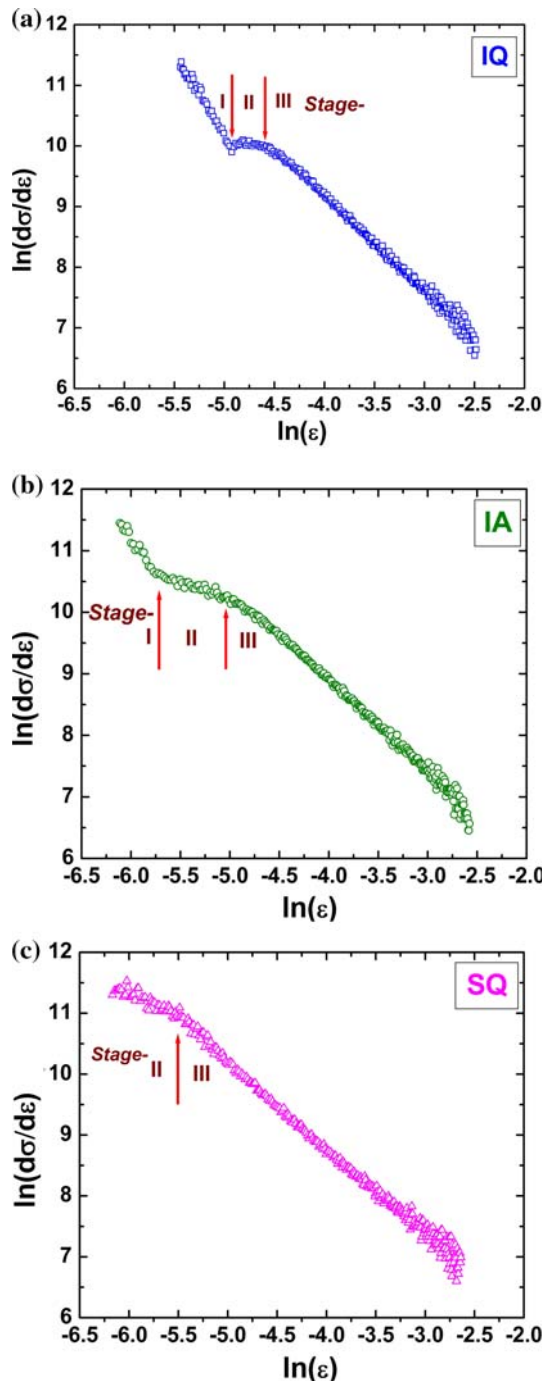


Fig. 5 Differential C-J plots of $\ln(d\sigma/d\varepsilon)$ versus $\ln(\varepsilon)$ for **a** IQ, **b** IA, and **c** SQ samples

allow one to infer that the amount of ferrite/austenite interfaces, and hence concentration of mobile dislocation in ferrite increases in the order of $IQ > IA > SQ$. Thus, the higher values of $(n' - 1)$ in stage-I and ε_t from stage-I to II (Table 3) for IQ sample than that for IA sample can be attributed to the differences in their microstructures in the two-phase region. The measured value of $(n' - 1)$ in stage-II for IQ sample is significantly higher than that of IA

sample, while stage-I and II overlap in SQ sample. In this context, Fig. 2 reveals that the largest length of the average ferrite grain in the microstructures decreases in the order of $IQ < IA < SQ$ treatment, and hence results in increasing order of constraint to the deformation of ferrite. The stage-III deformation is essentially dominated by the flow stress of martensite, which is comparable for the IQ, IA, and SQ samples having identical composition and comparable V_M . Therefore, it may be concluded that the D_{C-J} analysis allows to correlate the morphology of martensite at different levels of strain with the work-hardening behavior.

Modified C-J analysis

The modified C-J analysis [16, 18, 29] (M_{C-J}) of work-hardening is based on the Swift formula of stress-strain relationship expressed as [20]:

$$\varepsilon = \varepsilon_0 + c\sigma^m, \quad (4)$$

where ε_0 and c are material constants, and m is the inverse of the work-hardening exponent. Equation 4 after differentiation with respect to σ is:

$$\ln\left(\frac{d\sigma}{d\varepsilon}\right) = (1 - m) \ln \sigma - \ln(cm) \quad (5)$$

Analysis of work-hardening behavior of the generated DP microstructures by M_{C-J} technique resulted into only two stages of work-hardening irrespective of the martensite morphology as shown in Fig. 6. Two stages of work-hardening by M_{C-J} technique have been demonstrated

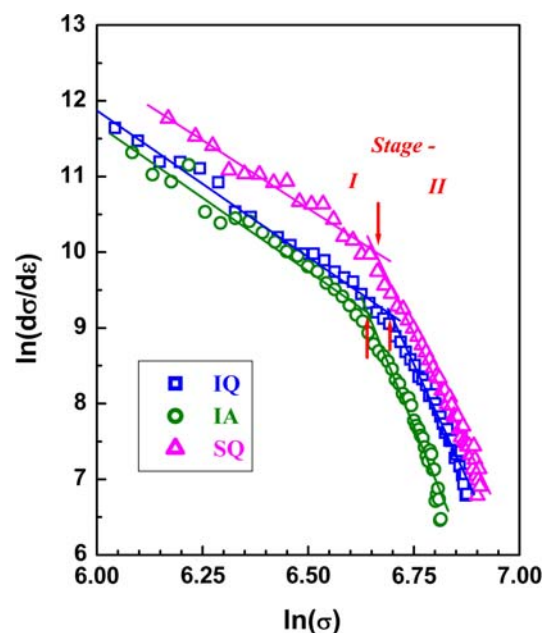


Fig. 6 Modified C-J plot of $\ln(d\sigma/d\varepsilon)$ versus $\ln(\sigma)$ of ferrite-martensite DP microstructures with varying morphology of martensite

earlier for DP steels with varying V_M [16, 17]. The two stages of work-hardening observed in this study as well as in earlier investigations are attributed to the following deformation mechanisms [3, 8, 16–18]:

- Stage-I: Deformation of soft ferrite matrix alone assisted by mobile dislocations present near the martensite regions.
- Stage-II: Uniform deformation of hard martensite and already work-hardened ferrite.

It is apparent that the values of $(1 - m)$ for all the three samples are comparable for both stage-I and II deformation (Table 3). However, the observed values of ϵ_t from stage-I to II according to M_{C-J} analysis (Table 3) vary significantly with the variation of martensite morphology and distribution. The results in Table 3 also indicate that the work-hardening of ferrite continues up to the level of strain which increases in the order of SQ, IA, and IQ treatments before the onset of work-hardening of martensite (Fig. 6).

Comparison of D_{C-J} and M_{C-J} analyses (Fig. 5 vis-à-vis Fig. 6) indicates that the M_{C-J} analysis essentially captures transition of work-hardening from ferrite dominated to martensite dominated regimes, whereas D_{C-J} analysis also reveals the intermediate stage of constrained plasticity of ferrite induced by hard martensite particles in the cases of IQ and IA samples. Thus it may be concluded that at the early stage of deformation of DP steel, the D_{C-J} analysis reveals the influence of martensite morphology on work-hardening more effectively than the M_{C-J} analysis. On the

other hand, the transition of work-hardening from the ferrite-dominated regime to the martensite-dominated regime is better revealed by the M_{C-J} analysis.

Analyses of fracture surface and sub-surface

With an aim to elucidate the effect of morphology and distribution of martensite on ductility, tensile fracture surfaces as well as sub-surfaces just beneath the fracture surface were studied under SEM for all of the heat-treated specimens. While fractographs reveal the fracture mechanisms, sub-surface micrographs provide better insight about the potential sites for the initiation of microvoids and/or microcracks. The representative fractographs and sub-surface microstructures of the investigated specimens are presented in Figs. 7 and 8. The fracture surfaces reveal mixture of cleavage facets and dimples for all the samples as shown in Figs. 7a and 8a, c. However, the area of cleavage surfaces increases in the order of SQ > IA > IQ, whereas the area of dimples increases in the reverse order. The size of the dimples is extremely fine for the IQ sample (Fig. 8a) as compared to IA sample (Fig. 8c), indicating the higher ductility of the former than the latter one. This is in agreement with the measured tensile ductility (Table 2). Fracture surface of the SQ sample exhibits predominantly cleavage nature (Fig. 7a) and is consistent with the earlier reports of similar microstructures [4, 10, 22, 30, 31].

Sub-surface micrograph of IA sample reveals the formation of microvoids at the ferrite/martensite interface

Fig. 7 SEM photographs of SQ sample: **a** tensile fracture surface, **b–d** microstructures of sub-surfaces close to the fracture surface. *Arrows* in **(b–d)** indicate the sites of cracks and/or voids nucleation. *M* martensite, *F* ferrite

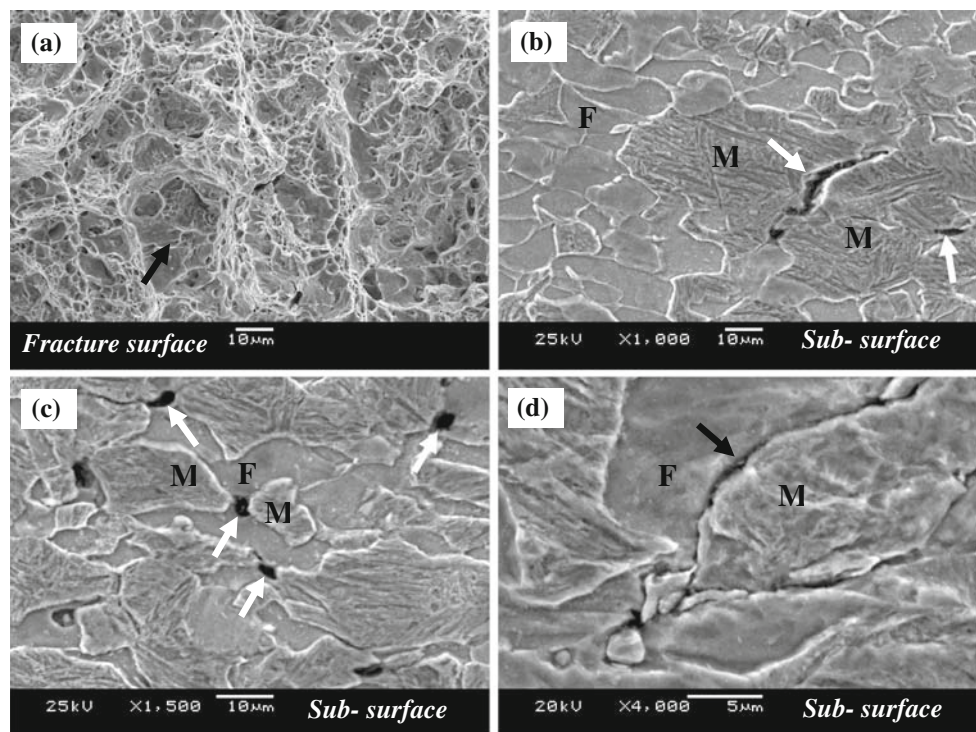
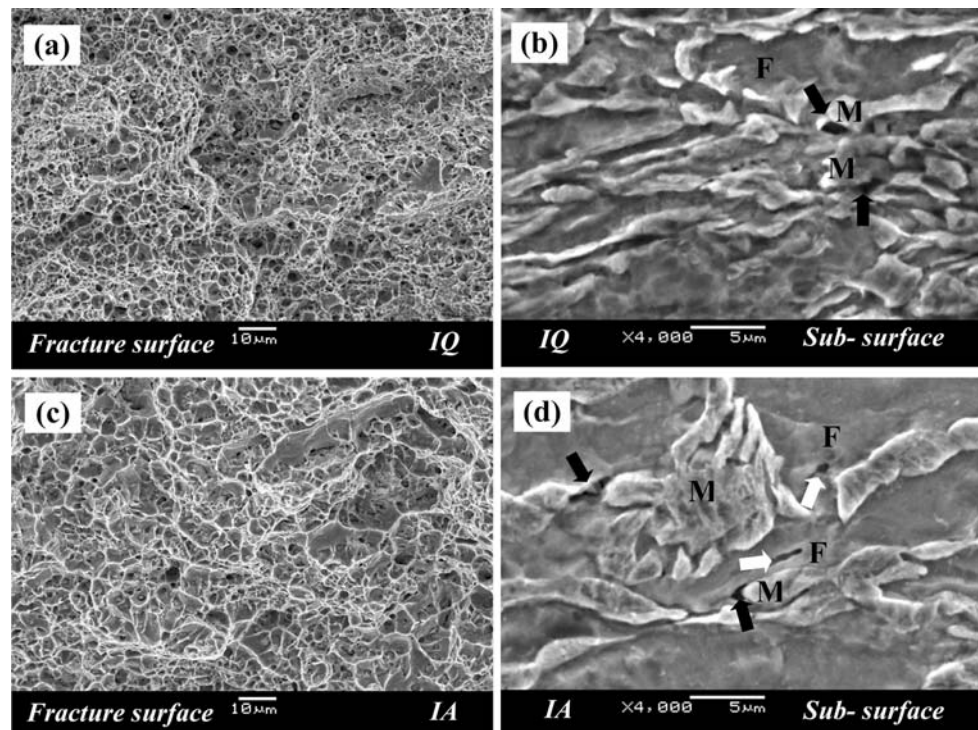


Fig. 8 SEM photographs of tensile fracture surfaces of **a** IQ and **c** IA samples, and sub-surface microstructures of **b** IQ and **d** IA samples. *Arrows* in **(b, d)** indicate the sites of void nucleation. *M* martensite, *F* ferrite



(marked by black arrows in Fig. 8d) as well as within the ferrite grains (marked by white arrows in Fig. 8d). In contrast, sub-surface micrograph of IQ sample shows the nucleation of microvoids only at the ferrite/martensite interfaces, mainly at the edge tip of fine fibrous martensites as marked by black arrows in Fig. 8b. Presence of microvoids within the ferrite grains for IA sample and absence of same for IQ sample allows one to infer that the ferrite phase is effectively restrained against plasticity by the surrounding martensite in IA sample, unlike that in IQ sample [2, 10, 31, 32]. This observation corroborates well with their mechanical properties (Table 2) and work-hardening behavior (Table 3). In the case of IQ sample, finer and random distribution of martensites having fibrous morphology restrict the growth of microvoids as they encounter the frequent discontinuities in the ferrite/martensite interfaces which delay the void coalescence resulting into higher values of elongation to failure. In the case of IA sample, the microvoids formed at martensite/ferrite interfaces can easily grow along the interface continuously due to the fact that such interfaces are having higher concentration of transformation strain and are nearly continuous, particularly for DP steels with higher V_M . These observations corroborate the fact that the ductility for IQ microstructure is much higher than that for IA microstructure at comparable level of V_M .

Sub-surface micrographs of SQ specimen demonstrate the frequent nucleation of microvoids at the ferrite/

martensite interfaces (Fig. 7c) as well as nucleation and propagation of microcracks within the martensite block (Fig. 7b). Formation of microcracks by fracturing of martensite particles has also been reported earlier in DP steels [6, 10, 29, 30, 32, 33]. Figure 7d shows that the interfaces of ferrite/martensite have opened up and martensite blocks are ready to be pulled out. Such pull out of martensite bands have resulted into the formation of domains of depression in the fracture surface of SQ specimen as marked by black arrow in Fig. 7a. Unlike SQ sample (Fig. 7), no microcracks were observed in the sub-surface microstructures of IQ and IA samples (Fig. 8). In addition, microvoids are much finer and fewer in number in the IQ and IA samples as compared to SQ sample. Moreover, microvoids in the IQ or IA samples are elongated toward the tensile loading direction, whereas the same in SQ sample appears nearly spherical. These observations indicate that SQ specimen undergoes much lower elongation before fracture than that for IQ and IA specimens and also substantiates that the magnitude of work-hardening of SQ sample is much lower compared to that for IQ and IA samples.

Therefore, correlation of work-hardening behavior and examinations of the features of fracture surface and sub-surface with different martensite morphologies in this study suggest that the microstructure of IQ sample is conspicuously the most preferred to obtain the best combination of strength-ductility in the high martensite regime of DP steel.

Conclusions

The results obtained in this study allow to draw the following major conclusions:

1. In the present high martensitic DP steel ($V_M \approx 0.32$), fine and fibrous martensite morphologies obtained by IQ treatment provided the best combination of strength and ductility along with lowest yield ratio and highest magnitude of work-hardening as desired for DP steels. Thus, the IQ treatment allows to circumvent the brittleness usually encountered in high martensitic DP steels.
2. The results suggest that the influence of martensite morphology on work-hardening of DP steel is better revealed in the D_{C-J} analysis than the M_{C-J} analysis at the early stage of deformation, whereas the transition of work-hardening from the ferrite-dominated regime to martensite-dominated regime is better delineated in the M_{C-J} analysis.
3. Analyses of tensile fracture surfaces and sub-surfaces have revealed that ferrite/martensite interfaces are most susceptible for microvoids nucleation. However, continuity of the ferrite–martensite interface rather than the amount of interface is responsible for growth/propagation of microvoids/microcracks.
4. Unlike IQ specimen, the microcracks are nucleated by the fracture of martensite in SQ specimen, whereas microvoids are also nucleated within the ferrite grain in the case of IA specimen, which corroborates the constrained imposed by the martensite in ferrite matrix.

References

1. Piplani RK, Raghavan V (1981) Steel India 4:1
2. Speich GR (1981) In: Kot RA, Bramfitt BL (eds) Fundamentals of dual phase steels. AIME, New York, p 1

3. Jiang Z, Lian J, Guan Z (1995) Mater Sci Eng A190:55
4. Davies RG (1979) Metall Trans A 10:113
5. Bag A, Ray KK, Dwarakadasa ES (1999) Metall Trans A 30:1193
6. Byun TS, Kim IS (1993) J Mater Sci 28:2923. doi:10.1007/BF00354695
7. Koo JY, Young MJ, Thomos G (1980) Metall Trans A 11:852
8. Tomita Y (1990) J Mater Sci 25:5179. doi:10.1007/BF00580148
9. Sankar S, Sangal S, Padmanabhan KA (2005) Mater Sci Technol 21:1152
10. Erdogan M (2002) J Mater Sci 37:3623. doi:10.1023/A:1016548922555
11. Hollomon JH (1945) Trans AIME 162:268
12. Crussard C (1953) Rev Metall 10:697
13. Jaoul B (1957) J Mech Phys Solids 5:95
14. Monteiro SN, Reed-Hill RE (1971) Met Trans 2:2947
15. Mamos LF, Matlock DK, Krauss G (1979) Metall Trans A 10:259
16. Samuel FH (1987) Mater Sci Eng 92:L1
17. Jha BK, Avtar R, Dwivedi VS, Ramaswamy V (1987) J Mater Sci Lett 6:891
18. Jiang Z, Jian L, Chen J (1992) Mater Sci Tech 8:1075
19. Ludwik P (1909) Element der Technolnischen Mechanick. Springer, Berlin, p 32
20. Swift HW (1952) J Mech Phys Solids 1:1
21. Kang S, Kwon H (1987) Metall Trans A 18:1587
22. Das P, Chattopadhyay PP, Bandyopadhyay NR (2003) J Met Mater Eng 84:84
23. Gural A, Tekeli S, Ando T (2006) J Mater Sci 41:7894. doi:10.1007/s10853-006-0871-4
24. Chunling Z, Dayong C, Bo L, Tianchen Z, Yunchang F (2004) J Mater Sci 39:4393. doi:10.1023/B:JMSC.0000033436.06575.aa
25. Soto R, Saikaly W, Bano X, Issartel C, Rigaut G, Charai A (1999) Acta Mater 47:3475
26. Wang ZG, Al SH (1999) ISIJ Int 39:747
27. Kim NJ, Thomas G (1981) Metall Trans A 12:483
28. Bayram A, Uguz A, Murat U (1999) Mater Charact 43:259
29. Umamoto M, Tsuchiya K, Liu ZG, Sugimoto S (2000) Metall Trans A 31:1785
30. Tomita Y, Okabayashi K (1985) Metall Trans A 16:73
31. Sarwar M, Priestner R (1996) J Mater Sci 31:2091. doi:10.1007/BF00356631
32. Nam WJ, Bae CM (1999) J Mater Sci 34:5661. doi:10.1023/A:1004705705208
33. Ahmad E, Sarwar M, Manzoor T, Hussain N (2006) J Mater Sci 41:5417. doi:10.1007/s10853-006-0266-6